RSC Advances

PAPER

View Article Online
View Journal | View Issue

Cite this: *RSC Adv.*, 2020, **10**, 19997

Highly-controllable drug release from core cross-linked singlet oxygen-responsive nanoparticles for cancer therapy†

Jiayan Zhou, Chunyang Sun * and Chunshui Yu *

Highly-controllable release consisting of preventing unnecessary drug leakage at physiologically normal tissues and triggering sufficient drug release at tumor sites is the main aim of nanoparticle-based tumor therapy. Developing drug-conjugation strategies with covalent bonds in response to a characteristic stimulus, such as reactive oxygen species (ROS) generated by photodynamic therapy (PDT) has attracted much attention. ROS can not only cause cytotoxicity, but also trigger the cleavage of ROS-responsive linkers. Therefore, it is feasible to design a new model of controlled drug release *via* the breakage of ROS-responsive linkers and degradation of nanoparticles. The self-supply of the stimulus and highly-controllable drug release can be achieved by encapsulation of photosensitizer (PS) and chemotherapeutic drugs simultaneously without any support of tumor endogenous stimuli. Therefore, we used thioketal (TK) linkers as the responsive linkers due to their reaction with singlet oxygen ($^1O_2$, SO), a type of ROS. They were conjugated to the side groups of polyphosphoesters (PPE) *via* click chemistry to acquire the core cross-linked SO-responsive PPE nanoparticles poly(thioketal phosphoesters) (TK-PPE). TK-PPE coated with the photosensitizer chlorin e6 (Ce6) and chemotherapeutic drug doxorubicin (DOX) simultaneously were prepared and named as TK-$PPE_{Ce6\&DOX}$. TK-$PPE_{Ce6\&DOX}$ kept stable due to the high stability of the TK-linkers in the normal physiological environment. With self-production of SO as the stimulating factor from the encapsulated Ce6, highly-controlled drug release was achieved. After incubation of tumor cells, 660 nm laser irradiation induced SO generation, resulting in the cleavage of TK-linkers and boosted-release of DOX. Highly-controllable drug release of TK-$PPE_{Ce6\&DOX}$ through self-production of stimulus increased antitumor efficacy, offering a promising avenue for clinical on-demand chemotherapy.

Received 4th March 2020
Accepted 14th May 2020

DOI: 10.1039/d0ra02053b

rsc.li/rsc-advances

1. Introduction

As an emerging non-invasive tumor treatment, nanoparticle-based photodynamic therapy has incorporated nanotechnology into traditional photodynamic therapy (PDT) to enhance the therapeutic effect.[1] Since most photosensitizers (PSs) are hydrophobic and poorly water-soluble, nanotechnology can be used to increase the solubility of PSs, so that the circulation time could be prolonged through physical loading and chemical bonding.[2–4] Furthermore, nanoparticle based-PSs can accumulate at the tumor site due to the ability of passing through the tumor neovascularized walls and reduced lymphatic drainage.[5,6] The phenomenon has been called the enhanced permeation and retention (EPR) effect. It should be noted that nanoparticles can be further modified with biological ligands, such as antibodies or peptides, to acquire the targeted ability towards tumors.[7] In addition, nanoparticle-based PDT could be incorporated into classical chemotherapy as well. The severe side effects of normal organs and tissues caused by chemotherapy are minimized, and chemotherapeutic drug-resistant tumor cells are able to be treated effectively by nanoparticle-based PDT because there is no cross resistance between PDT and chemotherapy. In this field, Li *et al.* designed a biocompatible theranostic nanoparticles poly(vinyl alcohol)-porphyrin (PPNs) based on the conjugation of photosensitizer pyropheophorbide a and poly(vinyl alcohol) (PVA). Chemotherapeutic drug doxorubicin (DOX) were encapsulated into PPNs subsequently. The treatment effect of the combination of PDT and chemotherapy was proved by *in vivo* antitumor efficacy. Tumor volumes of DOX loaded-PPNs group were reduced significantly after irradiation in comparison with control groups, and the mice survival rates of DOX loaded-PPNs were almost up to 80% after treatment for 40 days.[8] Lin and colleagues prepared a novel nanoscale coordination polymer (NCP)-based nanoparticles encapsulating with cisplatin as chemotherapeutic drug and pyrolipid as PS, named as NCP@pyrolipid, for the combination of

Department of Radiology and Tianjin Key Laboratory of Functional Imaging, Tianjin Medical University General Hospital, Tianjin 300052, P. R. China. E-mail: chysunshine@gmail.com; chunshuiyu@tmu.edu.cn

† Electronic supplementary information (ESI) available. See DOI: 10.1039/d0ra02053b

chemotherapy and PDT to treat resistant head and neck tumors. Results of *in vivo* antitumor efficacy demonstrated that NCP@pyrolipid had significant tumor inhibition in cisplatin resistant SQ20B tumors, while the mono-chemotherapy or mono-PDT could not achieve the same anti-tumor efficacy.[9]

Physical encapsulation and chemical conjugation are two main methods for drug encapsulation. However, hardly can common nanoparticles achieve highly-controlled drug release at tumor sites because of unnecessary leakage of encapsulated drugs during blood circulation. Therefore, the covalent coupling of drug molecules and nanocarriers through stimulus-responsive linkers allows nanoparticles to remain stable in the blood circulation, but degradation occurs in the responsive environment to achieve controlled drug release.[10] In terms of responsive-linkers, most studies focused on endogenous stimulus from tumor microenvironment, such as the intracellular reducing environment, endo/lysosomal acidic environment, and specific intracellular enzymes.[11] For instance, Zhang and coworkers prepared a redox-sensitive nanocarriers based on ditelluride-containing poly(ether-urethane) copolymers to achieve controlled release under abundant glutathione (GSH) conditions.[12] Chen *et al.* designed a novel pH-activated and size-changed nanoparticles which were composed of polyethylene glycol (PEG)-benzoic imine-oligo-L-lysine/iridium(III) metallodrug complex. Under acidic tumor microenvironments, nanoparticles could be changed into smaller ones for subsequent antitumor efficacy, because of the breakage of the pH-responsive benzoic imine bond.[13] However, it is hardly to ensure that endogenous stimulating factors always keep steady during the entire metabolic process of tumors. Consequently, it is likely to cause instability of release and unpredictable therapeutic efficacy. For example, the expression of some characteristic enzymes in tumors was significantly heterogeneous, resulting in endogenous stimulators changed across patients and stages of tumors.[14,15] Highly-controllable cleavable linkers are still in sore need of achieving precisely controlled drug release.

Long-wavelength light at 650–950 nm has been widely used in PDT, because of its deeper penetration, wider treatment range and fewer side effects in comparison with short-wavelength light.[16] In the process of long-wavelength light triggered PDT, oxygen could transform into cytotoxic reactive oxygen species (ROS), and ROS-responsive linkers, such as thioketal (TK) linkers, phenylboronic ester and di-selenide bonds could be cleaved in the sufficient oxygen environment.[17–21] Therefore, it is feasible to design a new model of controlled drug release *via* the breakage of ROS-responsive linkers and degradation of nanoparticles. Furthermore, the self-supply of the stimulus and highly-controllable drug release can be achieved by encapsulation of PS and chemotherapeutic drugs simultaneously because the ROS-sensitive nanoparticle could provide stimulus by itself and was independent of environmental stimuli. In this study, the biodegradable PEGylated polyphosphoester (PPE) was synthesized by the ring-opening polymerization (ROP) of 2-(but-3-yn-1-yloxy)-2-oxo-1,3,2-dioxaphospholane (BYP). TK-linkers were used as the responsive linkers. According to our previous study, it could react with singlet

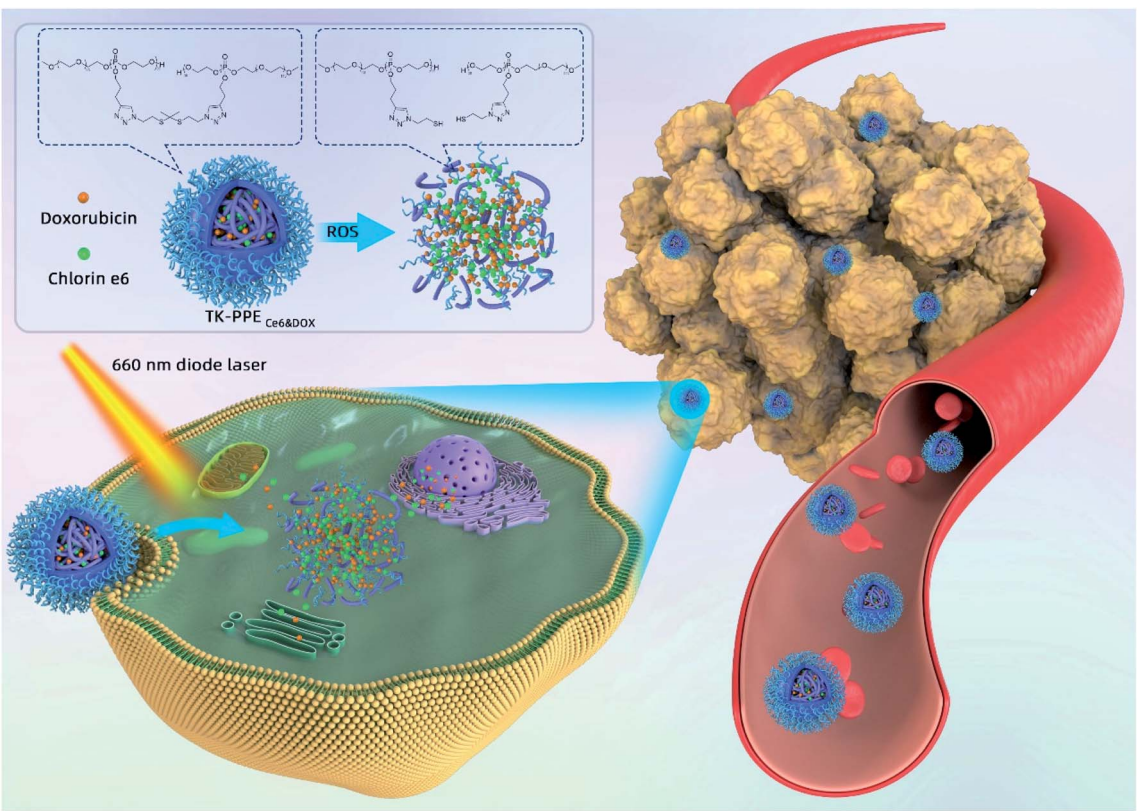

Scheme 1 Schematic illustration of TK-PPE$_{Ce6\&DOX}$ for photo-triggered chemotherapeutic drug release and cellular antitumor efficacy.

oxygen ($^1O_2$, SO), a type of ROS which generated by PDT type II reaction.[22] Subsequently, SO-sensitive TK-linkers were conjugated to the side groups of biodegradable PPE *via* click chemistry to form core-cross nanoparticles poly(thioketal phosphoesters) named as TK-PPE. The photosensitizer chlorin e6 (Ce6) and chemotherapeutic drug DOX were encapsulated into TK-PPE polymer to acquire TK-PPE$_{Ce6\&DOX}$ (Scheme 1). The circulation time of TK-PPE$_{Ce6\&DOX}$ could be prolonged because of the protection of PEG, and TK-PPE$_{Ce6\&DOX}$ could keep stable and prevent unnecessary drug release during blood circulation due to the stability of TK-linkers in physical condition. After the incubation of TK-PPE$_{Ce6\&DOX}$ into tumor cells, Ce6 was able to be photoactivated by 660 nm laser to generate a large amount of SO, then triggered TK-linkers to be cut *in situ*. The boosted release of DOX was allowed by the disassembly of TK-PPE to effective antitumor efficacy. In sum, TK-PPE$_{Ce6\&DOX}$ achieved self-sufficiency for highly-controllable release as it can provide the stimulating factor by itself, and the activation at the specific site had the potential for high-efficient killing ability towards the tumor.

2. Materials and methods

2.1 Materials

2-Chloro-2-oxo-1,3,2-dioxaphospholane (COP) was synthesized, distilled under vacuum and stored at −20 °C.[23] Tetrahydrofuran (THF) purchased from Alfa Aesar in Shanghai was used after distillation. After purification by phthalic anhydride, sodium hydroxide and calcium hydride, triethylamine (TEA, Aladdin) was distilled for subsequent studies. Monomethoxy poly(-ethylene glycol) (mPEG, $M_n = 5000$ g mol^{-1}) was acquired from Sigma-Aldrich and was dried by azeotropic distillation with toluene subsequently. 1,5,7-Triazabicyclo[4.4.0]dec-5-ene (TBD), anhydrous CH_2Cl_2, 3-butyn-1-ol, DOX and Ce6 were purchased from Sigma-Aldrich. All other undeclared reagents and solvents were of analytical grade and used as received.

2.2 Characterization

The proton nuclear magnetic resonance (^{1}H-NMR) spectra in $CDCl_3$ and deuterated dimethyl sulfoxide (DMSO-d_6) were recorded using a 400 MHz spectrometer (Avance III, Bruker, Germany). The infrared spectra of TK, PPE and TK-PPE were measured by Fourier Transform Infrared spectrometer (FT-IR spectrometer, ThermoFisher, China). The particle sizes of nanoparticles were determined at rt with the Malvern ZS90 dynamic light scattering instrument (Nano-ZS, Malvern instruments, UK). The UV-Vis characteristic absorption bands and drug loading contents (DLC) of nanoparticles were measured by the UV/Vis spectrophotometer (UV-3600 Shimadzu, Japan). The fluorescence of DOX was detected by the fluorescence spectrophotometer ($\lambda_{em} = 595$ nm, F-7000, Hitachi). The nanoparticle solution was taken in the screw capped quartz cuvettes for all UV-Vis and fluorescence measurement.

2.3 Cell line

The human breast adenocarcinoma (MCF-7) cells were acquired from American Type Culture Collection and cultured at 37 °C in Dulbecco's Modified Eagle's Medium (DMEM, Gibco, China) with 10% fetal bovine serum (FBS, Gibco, China) and 1% penicillin-streptomycin (Gibco, China) in the humidified 5% CO_2 incubator.

2.4 Synthesis of PPE

BYP was synthesized according to a previous study.[24] PPE was synthesized by the ROP of BYP, with TBD as organic catalyst and mPEG as macroinitiator. Typically, anhydrous mPEG (1.000 g, 0.20 mmol) and BYP (1.300 g, 8.03 mmol) were dissolved in anhydrous CH_2Cl_2 (3 mL) in a nitrogen-purified flask. After adding the catalyst TBD (0.0278 g, 0.20 mmol), the mixture was stirred for 20 min. The aforementioned reaction was performed at rt in the glovebox (Vigor, Suzhou) with water content below 0.1 ppm. The mixture was further purified by precipitation of cold diethyl ether/methanol mixture (10/1, v/v) twice, dried under vacuum and stored at −20 °C.

2.5 Preparation of DOX/Ce6-loaded nanoparticles

TK-PPE$_{Ce6\&DOX}$, TK-PPE$_{Ce6}$ and TK-PPE$_{DOX}$ were prepared by the nanoprecipitation method. Briefly, 10 mg of PEG–PBYP–N_3, 1 mg of DOX, 1 mg of Ce6 were dissolved in 1 mL of dimethyl sulfoxide (DMSO), and 10 mL of ultrapure water was added dropwise under stirring at rt. After stirring for 20 h, DMSO was removed by dialysis tube (Spectra/Por, Float-ALyzer, MWCO 3500) against ddH_2O. The unloaded DOX and Ce6 were removed by centrifugation at 3000 × *g* and filtration by 0.45 μm filter (Millipore). The resulted nanoparticles were denoted by TK-PPE$_{Ce6\&DOX}$. Ce6 or DOX were encapsulated solely by the same method as the controls, which were denoted as TK-PPE$_{Ce6}$ and TK-PPE$_{DOX}$. DLC and encapsulation efficiency (EE) of Ce6 and DOX were measured by the UV-Vis method at 660 nm and 495 nm which used in our previous study.[22,25,26] Nanoparticles were lyophilized and dissolved in DMSO. The following equations were used to calculate DLC and EE of Ce6 and DOX:

$$\text{DLC}\ (\%) = \frac{\text{amount of drug in nanoparticles}}{\text{amount of drug in nanoparticles} + \text{amount of nanoparticles}} \times 100\%$$

$$\text{EE}\ (\%) = \frac{\text{amount of drug in nanoparticles}}{\text{amount of total drug}} \times 100\%$$

2.6 *In vitro* measurement of ROS generation

The ROS generation was measured by a previously reported method.[27] TK-PPE$_{Ce6\&DOX}$ or TK-PPE$_{Ce6}$ ([Ce6] = 2 μg mL^{-1}) aqueous solution was irradiated (660 nm, 0.2 W cm^{-2}) for different time periods (0, 2, 4, 6, 8, 10 min). The absorbance of 1,3-diphenylisobenzofuran (DPBF) at 410 nm was recorded by UV/Vis spectrophotometer.

2.7 Degradation detection of TK-linkers

The cleavage of TK-linkers was detected by Ellman's test.[28] TK-$PPE_{Ce6\&DOX}$, TK-PPE_{Ce6} or TK-PPE_{DOX} ([DOX] = 6.17 μg mL^{-1}, [Ce6] = 2.90 μg mL^{-1}) in pH 8.0 phosphate buffer solution was irradiated with 660 nm laser (power density of 0.2 W cm^{-2}) for 0, 2, 4, 6, 8, 10 min. The absorbance of 5,5′-dithiobis (2-nitrobenzoic acid) (DTNB) at 412 nm was measured by UV/Vis spectrophotometer.

2.8 *In vitro* measurement of light-triggered DOX release

1 mL of TK-$PPE_{Ce6\&DOX}$ or TK-PPE_{DOX} ([DOX] = 61.7 μg mL^{-1}, [Ce6] = 29.0 μg mL^{-1}) aqueous solution was exposed to light (660 nm, 0.2 W cm^{-2}) at 0, 10, 20, 30, 40, 50, 60 min. The solutions of nanoparticles were transferred into 4 mL amicon ultra (Millipore, 10 KD) and were conducted with centrifugation (10 000 rpm, 20 min) by the high speed refrigerated centrifuge (Cence, China) to acquire free DOX solution. The collected solution of free DOX was lyophilized and dissolved with 1 mL DMSO. Fluorescence measurement was conducted to measure the concentration of released DOX, and the release measurements of all groups were conducted for three times with standard deviations in the dark environment.

2.9 Cellular uptake of nanoparticles

MCF-7 cells were seeded in 6-well plates (5×10^5 cells per well) and incubated at 37 °C overnight. The cell medium was replaced with fresh DMEM medium containing TK-$PPE_{Ce6\&DOX}$ or TK-PPE_{DOX} for further incubation of 2 h or 4 h. Then, cells were washed twice, trypsinized and centrifuged. The final cell suspensions were measured by the flow cytometer (BD AccuriC6, USA), and results were analyzed by FlowJo® V10 software.

2.10 Observation of intracellular generation of ROS

MCF-7 cells were seeded in 35 mm glass bottom dishes (5×10^5 cells per dish) and cultured at 37 °C overnight. Then, cells were treated with fresh DMEM medium embracing TK-$PPE_{Ce6\&DOX}$, TK-PPE_{Ce6} or TK-PPE_{DOX} ([Ce6] = 2.50 μg mL^{-1}) for 4 h. After removing nanoparticles, cells were incubated with 2′-7′-dichlorodihydrofluorescein diacetate (DCFH-DA, λ_{ex} = 488 nm) for another 30 min and irradiated with laser (660 nm, 0.2 W cm^{-2}, 15 min) subsequently. The results were observed by confocal laser scanning microscope (CLSM, Leica, USA).

2.11 Intracellular DOX release triggered by laser

MCF-7 cells were seeded in 35 mm glass bottom dishes at a density of 5×10^5 cells per dish and were incubated at 37 °C for 24 h. The culture medium was replaced with fresh DMEM medium including TK-$PPE_{Ce6\&DOX}$ or TK-PPE_{DOX} ([DOX] = 2 μg mL^{-1}) for 4 h. Then, cells were washed with phosphate buffer saline (PBS), irradiated with laser (660 nm, 0.2W cm^{-2}, 30 min) and cultured for 2 h. After fixed in 4% paraformaldehyde, F-actin and cell nucleus were counterstained with Alexa Fluor 488 phalloidin (λ_{ex} = 488 nm) and 4′,6-diamidino-2-phenylindole (DAPI, λ_{ex} = 358 nm) according to manufacturer's instructions for CLSM (Leica, USA) observation.

2.12 Apoptosis assay

MCF-7 cells were seeded in 6-well plates (5×10^5 cells per well) and incubated at 37 °C overnight. The cell medium was replaced with fresh DMEM medium containing TK-$PPE_{Ce6\&DOX}$, TK-PPE_{Ce6} or TK-PPE_{DOX} ([DOX] = 0.5 μg mL^{-1}) for 4 h. Cells were washed twice, irradiated with laser (660 nm, 0.2 W cm^{-2}, 30 min) and cultured for another 20 h. Following the annexin V-FITC apoptosis detection kit (Beyotime Biotechnology, China) procedure, cell suspensions were counterstained with fluorescein isothiocyanate (FITC)-labeled annexin V and propidium iodide (PI). The results were analyzed by FlowJo® V10 software.

2.13 *In vitro* cytotoxicity

Calcein-AM/PI Double Staining were carried out primarily to verify the cell viability. MCF-7 cells were seeded in 35 mm glass bottom dishes (4×10^5 cells per dish) and incubated at 37 °C overnight. The subsequent procedures of incubation and irradiation were consistent with that of annexin V-FITC apoptosis detection as described above, and the experimental concentration of DOX was 2 μg mL^{-1}. Live cells and dead cells were counterstained with calcein-AM (λ_{ex} = 488 nm) and PI (λ_{ex} = 535 nm) according to manufacturer's instructions (Keygen, China) for CLSM (Leica, USA) observation. Furthermore, the quantitative therapeutic efficacy was evaluated by the standard cell-counting kit 8 (CCK-8) assay. MCF-7 cells were seeded in 96-well plates at 5×10^3 cells with 100 μL medium per well overnight. TK-$PPE_{Ce6\&DOX}$, TK-PPE_{Ce6} or TK-PPE_{DOX} nanoparticles at 0.5, 1, 2 μg mL^{-1} concentration of DOX were added and were internalized for 4 h. Afterward, cells were irradiated with laser (660 nm, 0.2 W cm^{-2}, 30 min) and cultured for another 20 h or 68 h. 10 μL of CCK-8 (MedChem Express, China) were added into per well to assess the cell viability followed by the standard protocol.

2.14 Statistical analysis

The statistical significance of the above results was assessed through Student's *t*-test (two-tailed); $p < 0.05$ was considered statistically significant in all analyses (95% confidence level).

3. Results and discussion

3.1 Preparation and characterization of TK-$PPE_{Ce6\&DOX}$

The ROP was commonly used for polymerizing cyclic phosphoesters into linear PPE. By investigation of catalysts, the controllable synthesis of PPE *via* the ROP had made great progress. As the common metal catalysts in the ROP, aluminum triisopropoxide and stannous octoate could catalyze the ROP of PPE with controllability.[29,30] However, its potential biological toxicity limited its biological applications. Iwasaki *et al.* studied the ROP of PPE by TBD or 1,8-diazabicyclo[5.4.0]undec-7-ene (DBU) as organic catalysts to overcome the above disadvantage. The degree of polymerization was in proportion to the conversion of the monomer within certain limits, while the dispersion of PPE remained unchanged.[31] Nowadays, PPE were commonly synthesized by the ROP with organic catalysts. Wooley *et al.* applied DBU as the catalyst and benzyl alcohol as

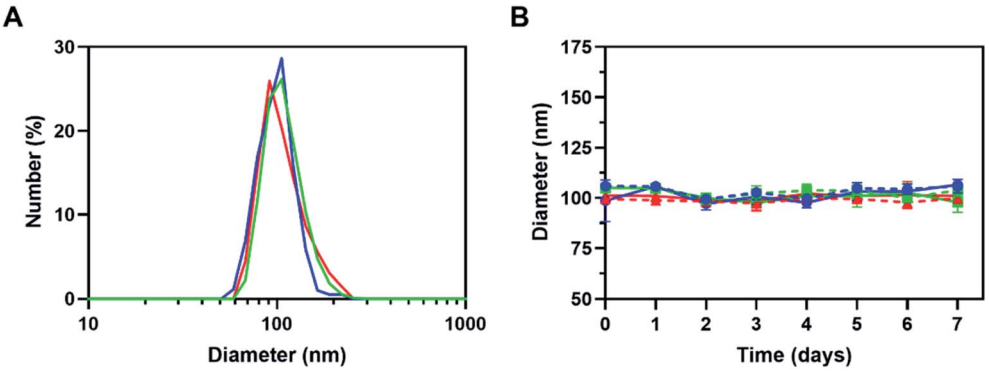

Fig. 1 Particle sizes (A) and stability for 7 days (B) of TK-PPE$_{Ce6}$ (green), TK-PPE$_{DOX}$ (red) and TK-PPE$_{Ce6\&DOX}$ (blue). Full lines and dotted lines stand for PBS and PBS containing 10% FBS solution respectively.

the initiator to synthesize poly(2-(but-3-yn-1-yloxy)-2-oxo-1,3,2-dioxaphospholane) (PBYP) for further click chemistry reaction.[32] Ni *et al.* synthesized the diblock PPE containing alkynyl group to conjugate folate acid as well as azide-modified cross-linkers N_3-*a*-TEG-*a*-N_3.[33] In this study, PPE was synthesized by the ROP of BYP, with the organic catalyst TBD and macro-initiator mPEG. The main characteristic resonance of PEG segment could be found at δ 3.36–3.39 ppm (peak a) and δ 3.60–3.70 ppm (peak b) (Fig. S1A†).[32,33] The resonances at δ 2.56–2.67 ppm (peak c) and δ 2.04–2.17 ppm (peak d) were assigned to the protons of methylene beside the alkynyl group (–CH_2C≡CH) and alkynyl group (≡CH) of PBYP, respectively (Fig. S1A†). These results proved the successful synthesis of PPE. Click chemistry, also named as link chemistry, were came up with K. Barry Sharpless in 2001. The main purpose was to achieve the chemical synthesis of various molecules quickly through the splicing of small units. It particularly emphasized the development of new combinatorial chemistry methods based on carbon–heteroatom bond (C–X–C) synthesis to obtain diverse molecules simply. Azide–alkyne Huisgen cycloaddition was the representative reaction of click chemistry. Azide group remained stable in normal condition, however it could be reacted with terminal alkynes to generate 1,3-substituted triazoles efficiently with monovalent copper catalyst.[34,35] Therefore, the occurred azide–alkyne Huisgen cycloaddition between the alkynyl groups of PPE and the azide groups of TK-linkers could form the core-cross micelles TK-PPE. The PBYP segments were presented in the core through the introduction of the cross-linking bridges *via* click chemistry, and the acquired TK-PPE micelles could have more cross-linking inside core to keep more stable. The core cross-linking not only prevented the dissociation of micelles at a low concentration, but it was reversible to be cleaved as well because of the SO sensitive-crosslinker TK-linkers.[36,37] TK-PPE was dissolved in DMSO-d_6 to verify its synthesis through ^{1}H-NMR spectrum (Fig. S1B†). The characteristic resonance of PEG had little displacement caused by the use of different solvents. There were only hydrophilic proton peaks of PEG without peak c, d (Fig. S1A†) of PPE appeared in the ^{1}H-NMR spectrum. The formed covalent bonds between the PBYP segments lead to the rigid hydrophobic core after click chemistry. The solvent could not penetrate the inside of the core, so that the micellar structure could maintained in organic solvents, and the signal corresponding to the strength of the internal PBYP segments could not be demonstrated.[37] FT-IR spectrometer was used to determine the successful synthesis of TK-PPE as well. Azido groups and alkynyl groups owned its characteristic absorption peaks (2160–2100 cm^{-1} and 2300–2100 cm^{-1}) in infrared spectrum. As shown in Fig. S2,† it could

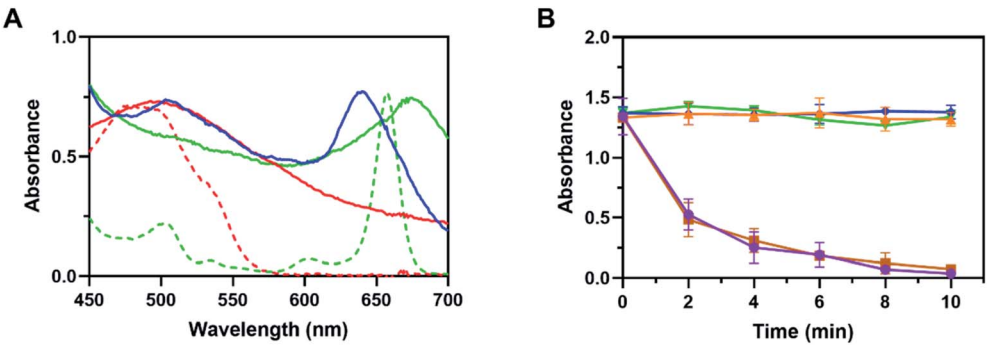

Fig. 2 (A) The UV-Vis absorption spectra of free Ce6 (green dot line), free DOX (red dot line), TK-PPE$_{Ce6}$ (green), TK-PPE$_{DOX}$ (red) and TK-PPE$_{Ce6\&DOX}$ (blue). (B) The UV-Vis absorbance of DPBF at 410 nm of nanoparticles under irradiation (660 nm, 0.2 W cm^{-2}). TK-PPE$_{Ce6}$: green inverted triangle; TK-PPE$_{Ce6}$ + L: brown square; TK-PPE$_{DOX}$ + L: orange triangle; TK-PPE$_{Ce6\&DOX}$: blue rhombus; TK-PPE$_{Ce6\&DOX}$ + L: purple circle.

be clearly observed that the appearance of the absorption peak at 2100 cm^{-1} of azide groups from TK-linkers and 2300 cm^{-1} of alkynyl groups of PPE, and the vanishing of these characteristic peaks of TK-PPE demonstrated the click chemistry reaction between PPE and TK-linkers happened which was in accordance with previous studies.[38,39]

The photosensitizer Ce6 and chemotherapeutic drug DOX were loaded into TK-PPE polymer by the nanoprecipitation method to obtain TK-$PPE_{Ce6\&DOX}$.[17] Ce6 or DOX were encapsulated solely by the same method as the controls for subsequent experiments, which were denoted as TK-PPE_{Ce6} and TK-PPE_{DOX}. The average diameter of TK-$PPE_{Ce6\&DOX}$ was about 105 nm, and the sizes of TK-PPE_{Ce6} and TK-PPE_{DOX} were basically the same (Fig. 1A). Besides, the particle sizes of TK-$PPE_{Ce6\&DOX}$, TK-PPE_{Ce6} and TK-PPE_{DOX} remained stable in PBS and PBS containing 10% FBS at least during the first 7 days (Fig. 1B).

The size in nanoscale and stability were attributed to the core cross-linking structure as described above. The similar characteristic absorption bands at 495 nm of TK-$PPE_{Ce6\&DOX}$, TK-PPE_{DOX} and free DOX (Fig. 2A) demonstrated the successful encapsulation of DOX. Besides, the maximum absorption spectra of TK-$PPE_{Ce6\&DOX}$ (640 nm) and TK-PPE_{Ce6} (674 nm) which were around free Ce6 (660 nm) showed that Ce6 occurred slight redshift during encapsulation, suggesting the intermolecular π–π stacking interaction between Ce6 and DOX. Furthermore, the stability of nanoparticles improved at the same time due to this interaction as well.[40] The loading contents of Ce6 and DOX of TK-$PPE_{Ce6\&DOX}$ were up to 2.90% and 6.17%, respectively (Table S1†), which was similar to that of TK-PPE_{Ce6} and TK-PPE_{DOX}.

3.2 The mechanism of DOX release from TK-$PPE_{Ce6\&DOX}$ under irradiation

Based on our design, 660 nm laser could initiate photosensitizaton of TK-$PPE_{Ce6\&DOX}$, and generated ROS, prevalent SO, then triggered TK-linkers to be cut *in situ*. TK-$PPE_{Ce6\&DOX}$ dissociated then, and finally the encapsulated DOX released from the micelle core. Therefore, we first wondered whether the encapsulated Ce6 could be activated and produced SO by 660 nm laser. SO sensitive indicator DPBF which occurred decomposition reaction with SO were involved in the experiment.[41] The DPBF absorbance at 410 nm of TK-$PPE_{Ce6\&DOX}$, TK-PPE_{Ce6} and TK-PPE_{DOX} under laser were obtained for measuring the production of SO. As shown in Fig. 2B, the absorbance changes of DPBF in TK-PPE_{DOX} with light, TK-PPE_{Ce6} and TK-$PPE_{Ce6\&DOX}$ without light were negligible during irradiation (660 nm, 0.2 W cm^{-2}) because they cannot produce SO. In contrast, for TK-$PPE_{Ce6\&DOX}$ and TK-PPE_{Ce6} groups, laser irradiated for 2 min could result in sharp absorbance decreases of DPBF, and the absorbance almost reached zero after 10 min irradiation. Under 660 nm laser, the encapsulated Ce6 in TK-$PPE_{Ce6\&DOX}$ and TK-PPE_{Ce6} could be activated rapidly to generate SO.

The second question is whether the TK-linkers of TK-PPE could be cleaved by SO. TK-linkers would be broken and converted to thiol terminal groups after reaction with SO as previous studies. Ellman's test was commonly used to measure thiol terminal groups to reflect the cleavage of TK-linkers.[28] DTNB absorbance at 412 nm in TK-$PPE_{Ce6\&DOX}$ and TK-PPE_{Ce6} group increased constantly with irradiation (660 nm, 0.2 W cm^{-2}) from 0 to 10 min (Fig. 3A). By contrast, there was almost no change in absorbance of DTNB of TK-PPE_{DOX} and TK-$PPE_{Ce6\&DOX}$, TK-PPE_{Ce6} without illumination. Therefore, the cleavage of TK-$PPE_{Ce6\&DOX}$ and TK-PPE_{Ce6} with laser could be explained as TK-linkers only degraded by SO, and the encapsulation of Ce6 made it possible for SO to react with TK-linkers in its short action distance (<20 nm) and limited lifetime (<40 ns).[42]

We next investigated whether the dissociation of TK-PPE would stimulate the release of DOX. Fluorospectrophotometer was conducted for quantifying DOX cumulative release (λ_{em} = 595 nm) of TK-$PPE_{Ce6\&DOX}$ and TK-PPE_{DOX} with laser or not.[43] As illustrated in Fig. 3B, less than 10% of DOX released at 60 min in TK-PPE_{DOX} and TK-$PPE_{Ce6\&DOX}$ without laser. DOX release of TK-$PPE_{Ce6\&DOX}$ with illumination (660 nm, 0.2 W cm^{-2}) was rose significantly from 0 to 60 min. It could be clearly observed that the proportion of TK-$PPE_{Ce6\&DOX}$ (L+) cumulative DOX release in 60 min had a remarkable increase in comparison with the group

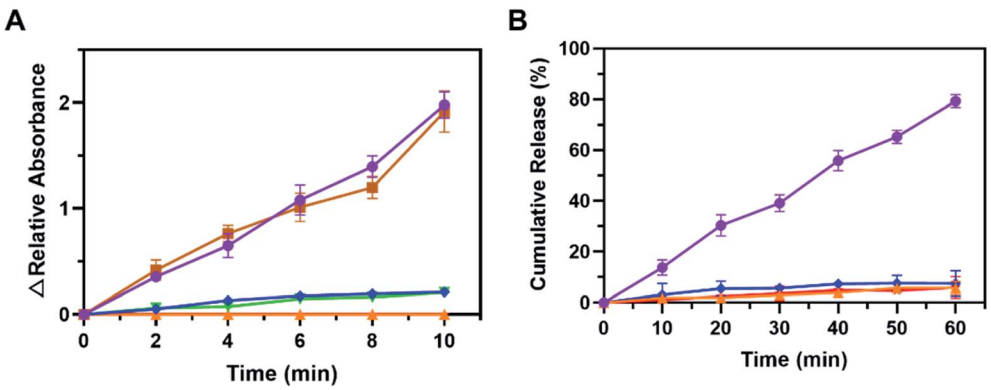

Fig. 3 (A) The UV-Vis changes of DTNB at 412 nm of TK-PPE_{Ce6}, TK-PPE_{DOX} and TK-$PPE_{Ce6\&DOX}$ with or without light irradiation (660 nm, 0.2 W cm^{-2}). (B) The cumulative release of DOX from TK-PPE_{DOX} and TK-$PPE_{Ce6\&DOX}$ with or without light irradiation (660 nm, 0.2 W cm^{-2}). TK-PPE_{Ce6}: green inverted triangle; TK-PPE_{Ce6} + L: brown square; TK-PPE_{DOX}: red star; TK-PPE_{DOX} + L: orange triangle; TK-$PPE_{Ce6\&DOX}$: blue rhombus; TK-$PPE_{Ce6\&DOX}$ + L: purple circle.

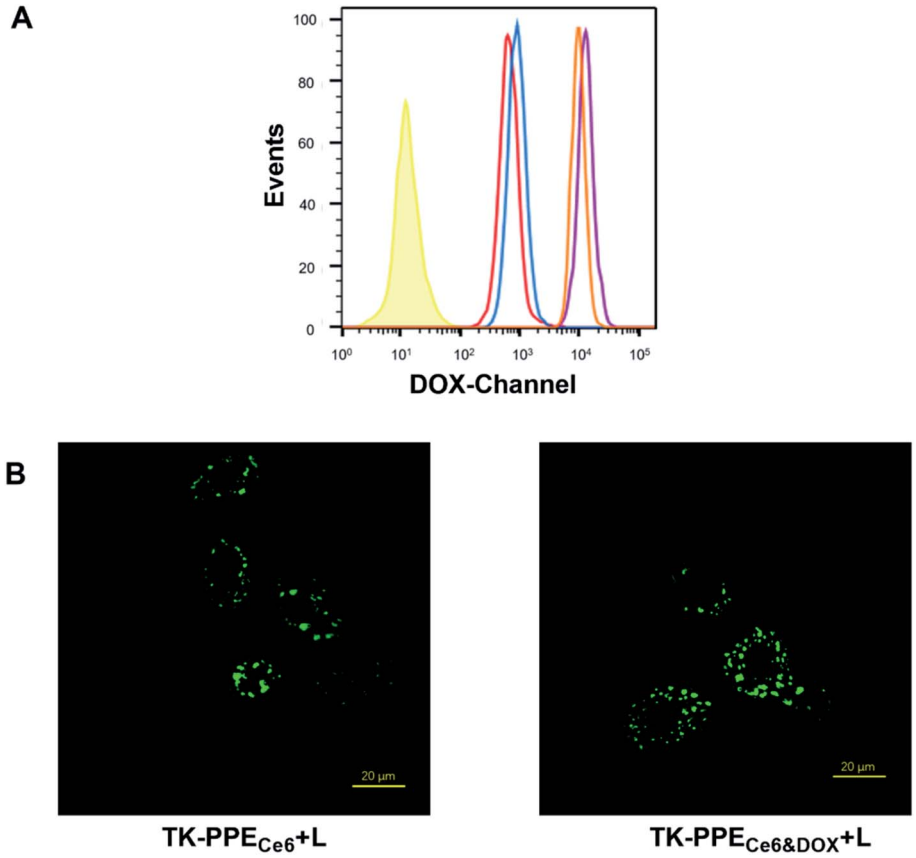

Fig. 4 (A) Flow cytometric analysis of the internalization of TK-PPE$_{Ce6\&DOX}$ and TK-PPE$_{DOX}$ by MCF-7 cells after 2 h and 4 h of incubation. From left to right: TK-PPE$_{DOX}$ incubated for 2 h (red), TK-PPE$_{Ce6\&DOX}$ incubated for 2 h (blue), TK-PPE$_{DOX}$ incubated for 4 h (orange), TK-PPE$_{Ce6\&DOX}$ incubated for 4 h (purple). (B) CLSM images of MCF-7 cells incubated with TK-PPE$_{Ce6}$ and TK-PPE$_{Ce6\&DOX}$ respectively, and then treated DCFH-DA, irradiated by 660 nm laser (0.2 W cm^{-2}, 15 min). The scale bar is 20 μm.

without light (79.8% *vs.* 7.8%), demonstrating the controlled-release ability of TK-PPE$_{Ce6\&DOX}$ under irradiation.

To sum up, the above results proved that TK-PPE$_{Ce6\&DOX}$ solution accomplished highly-controlled drug release by self-sufficiency. Typically, TK-PPE$_{Ce6\&DOX}$ could remain stable in solution and be photosensitized to produce SO rapidly by 660 nm laser irradiation, causing the cleavage of SO-responsive TK-linkers and dissociation of nanoparticles, thereby achieving boosted DOX release.

3.3 Light-triggered DOX release achieved significant lethality towards tumor

We also tested whether TK-PPE$_{Ce6\&DOX}$ achieved self-supply at the cellular level and exerted therapeutic effect of PDT and chemotherapy according to the above results of characterization. Primarily, the flow cytometry was used to verify the cellular uptake of TK-PPE$_{Ce6\&DOX}$ and TK-PPE$_{DOX}$. As shown in Fig. 4A, as the incubation time prolonged from 2 h to 4 h, the intracellular DOX fluorescence intensity of TK-PPE$_{Ce6\&DOX}$ increased, which were similar with that of TK-PPE$_{Ce6\&DOX}$. The aforementioned results demonstrated that more TK-PPE$_{Ce6\&DOX}$ or TK-PPE$_{DOX}$ could be internalized into cells with the extension of the culturing time.

Immunofluorescence images of MCF-7 cells with the internalization of DCFH-DA as the SO-sensitive fluorescent probe of various formations were obtained by CLSM. As shown in Fig. 4B and S3,† TK-PPE$_{Ce6\&DOX}$ and TK-PPE$_{Ce6}$ with irradiation (660 nm, 0.2 W cm^{-2}, 15 min) had green fluorescence within cells. On the contrary, cellular fluorescence signal was hardly to be found in TK-PPE$_{DOX}$, TK-PPE$_{Ce6\&DOX}$, TK-PPE$_{Ce6}$ without irradiation, indicating that TK-PPE$_{Ce6\&DOX}$ under irradiation could be photoactivated within cells as similar as *in vitro*.

Intracellular controlled DOX release stimulated by light-generated SO was also verified by CLSM. After being treated with TK-PPE$_{Ce6\&DOX}$ or TK-PPE$_{DOX}$ for 4 h, cells were stained with DAPI (blue) and Alexa Fluor 488 phalloidin (green) to locate cell nucleus and cytoskeleton. Intracellular DOX fluorescence (red) were recognized by its exciting light at 475 nm. As shown in Fig. 5 and S4,† there was no co-localization between blue and red fluorescent signals for cells treated with TK-PPE$_{DOX}$ and TK-PPE$_{Ce6\&DOX}$ without irradiation. After irradiation for 30 min, noticeable red DOX fluorescence of TK-PPE$_{Ce6\&DOX}$ could be found in the nucleus. As one of broad-spectrum antitumor drugs, DOX could inhibit the synthesis of nucleic acids and exert cytotoxic effect by embedding its DNA in the nucleus of tumor cells,[44] and the prerequisite for its antitumor effect was the intranuclear DOX. Therefore, the loaded DOX of TK-PPE$_{Ce6\&DOX}$ released and translocated into tumor cell nucleus due to the dissociation of TK-PPE$_{Ce6\&DOX}$

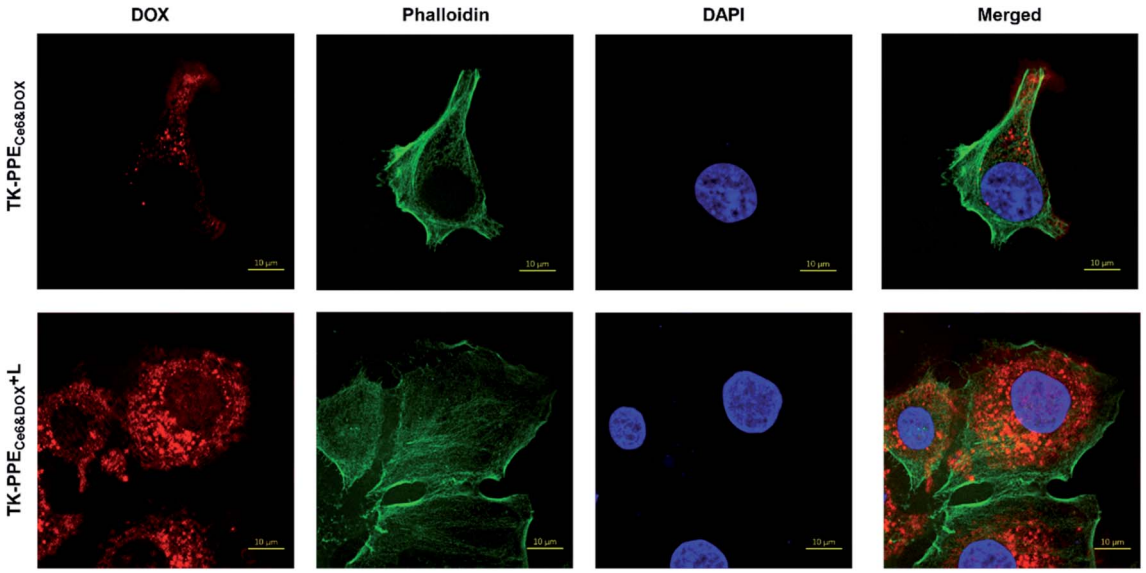

Fig. 5 Assessment of intracellular DOX release and biodistribution in MCF-7 cells of TK-PPE$_{Ce6\&DOX}$ with or without irradiation (660 nm, 0.2 W cm^{-2}, 30 min). Cell nucleus and F-actin were counterstained with DAPI (blue) and Alexa Fluor 488 phalloidin (green). The scale bar is 10 μm.

under irradiation. In contrast, great majority of TK-PPE$_{DOX}$ and TK-PPE$_{Ce6\&DOX}$ under dark condition stayed in the cytoplasm without DOX release.

It is reasonable that the increased DOX release from TK-PPE$_{Ce6\&DOX}$ might cause greater damage to tumor cells. According to the pharmacological mechanism of DOX

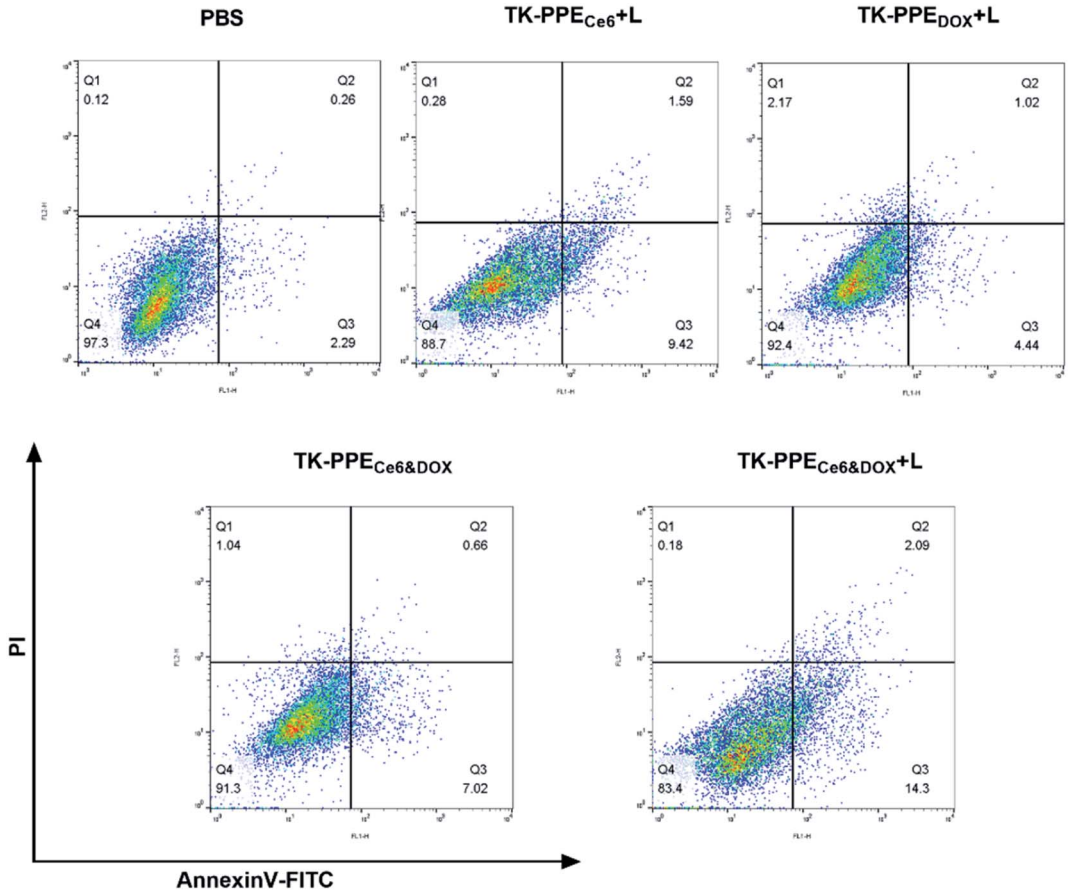

Fig. 6 Flow cytometry analysis of MCF-7 cell apoptosis induced by various formulations based on annexin V-FITC/PI staining. Early and late apoptotic cells were shown in the lower right quadrant and upper right quadrant, respectively.

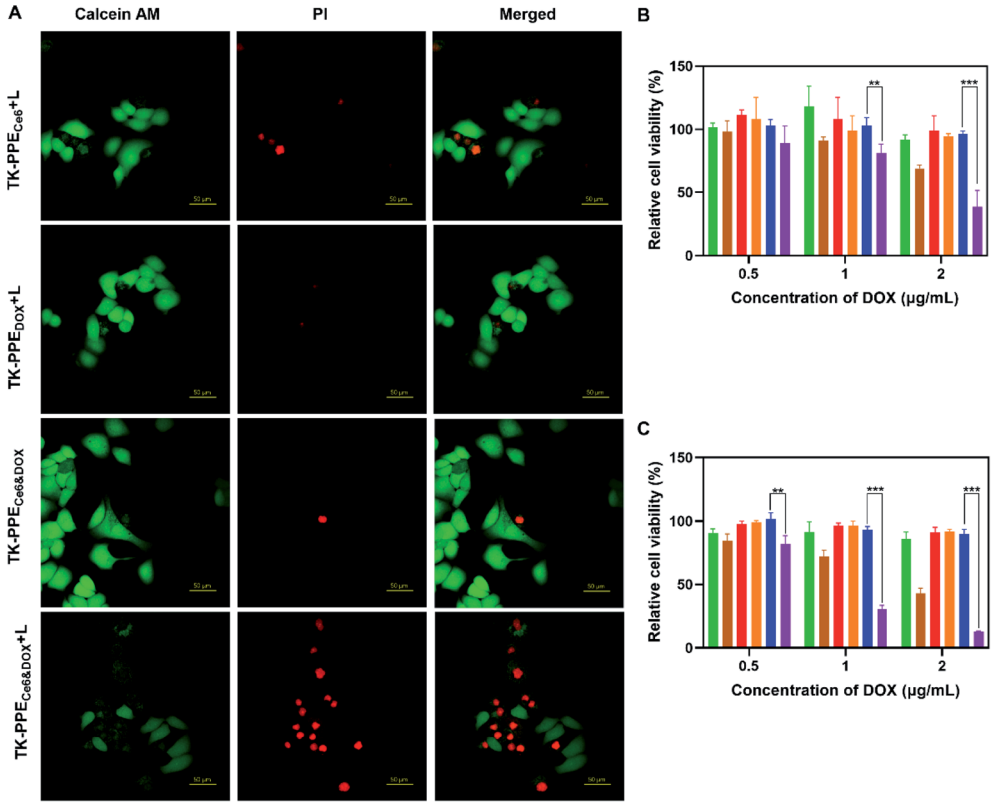

Fig. 7 (A) CLSM images of MCF-7 cells incubated with TK-PPE$_{Ce6}$, TK-PPE$_{DOX}$ and TK-PPE$_{Ce6\&DOX}$ respectively with or without light irradiation (660 nm, 0.2 W cm^{-2}, 30 min). Live cells and dead cells were counterstained with calcein-AM (green) and PI (red). The scale bar is 50 μm. Cytotoxicity of MCF-7 cells incubated with TK-PPE$_{Ce6}$, TK-PPE$_{DOX}$ and TK-PPE$_{Ce6\&DOX}$. The cells were treated with nanoparticles for 4 h. After irradiation (660 nm, 0.2 W cm^{-2}) for 30 min, the cells were further incubated with fresh medium for 20 h (B) or 68 h (C). TK-PPE$_{Ce6}$: green; TK-PPE$_{Ce6}$ + L: brown; TK-PPE$_{DOX}$: red; TK-PPE$_{DOX}$ + L: orange; TK-PPE$_{Ce6\&DOX}$: blue; TK-PPE$_{Ce6\&DOX}$ + L: purple. $^{**}p < 0.01$, $^{***}p < 0.005$.

consisting of inducing cell apoptosis and the cytostatic effect,[45] annexin V-FITC apoptosis detection, calcein-AM/PI double staining and CCK-8 assay were performed to prove the cell apoptosis and cell viability respectively. Firstly, the staining with annexin-V-FITC and PI were carried out, and the results were illustrated in Fig. 6. TK-PPE$_{Ce6\&DOX}$ + L showed the greatest ability of inducing cell apoptosis, which is up to 16.4%, with 14.3% of early apoptosis. TK-PPE$_{Ce6}$ + L led to moderate cell apoptosis because of the cytotoxic SO. On the other hand, the proportion of apoptotic cells of TK-PPE$_{DOX}$ + L and TK-PPE$_{Ce6\&DOX}$ without light were significantly lower than that of TK-PPE$_{Ce6\&DOX}$ + L. Early apoptosis was the most representative in cell apoptosis, because necrotic cells would be stained by annexin-V-FITC and PI as well, thereby counting in the late apoptotic quadrant.[46] Treatment with TK-PPE$_{Ce6\&DOX}$ + L had the highest apoptotic ratio, most of which were early apoptosis, demonstrating that the increased cell apoptosis was the result of PDT with photo-triggered chemotherapy.

Calcein-AM/PI double staining was performed to verify the cell viability. Calcein-AM (green) and PI (red) stand for living cells and dead cells respectively. Immunofluorescence images taken by CLSM were shown in Fig. 7A. After treatment with TK-PPE$_{Ce6\&DOX}$ under 660 nm laser irradiation, numerous damaged cells with strong red fluorescence could be observed, indicating the cytotoxicity caused by released DOX of TK-PPE$_{Ce6\&DOX}$ + L. The cell viability of TK-PPE$_{DOX}$ + L and TK-PPE$_{Ce6\&DOX}$ without laser was not obviously influenced indicated by significant green fluorescence. Furthermore, the quantitative therapeutic efficacy at 24 h and 72 h was evaluated by CCK-8 assay (Fig. 7B and C). For TK-PPE$_{Ce6\&DOX}$ (L−), TK-PPE$_{Ce6}$ (L−) and TK-PPE$_{DOX}$, there were only negligible cytotoxicity towards MCF-7 cells in the whole duration. On the other hand, TK-PPE$_{Ce6}$ under irradiation demonstrated moderate cytotoxicity because of the cytotoxic SO offered by the encapsulated Ce6. At 24 h and 72 h, the cell lethality of TK-PPE$_{Ce6\&DOX}$ plus light was always highest under all tested concentration, and its cell viability at 72 h were much lower than that of 24 h, only 13.7% of total cells survived after treating with 2 μg mL^{-1} of DOX concentration, suggesting the significant and continuous antitumor efficacy due to the therapeutic effect of PDT and photo-activated chemotherapy.

Altogether, TK-PPE$_{Ce6\&DOX}$ under laser could accomplish highly-controlled drug release with self-sufficiency at the cellular level as well. Effective and long-playing tumor cell inhibition were observed for the lethality of the released DOX and photocytotoxicity.

4. Conclusion

In summary, the SO-responsive nanoparticle TK-PPE$_{Ce6\&DOX}$ was developed for highly-controllable drug release in the tumor

cells by self-providing stimulus. The integrity of TK-$PPE_{Ce6\&DOX}$ in physiological condition was attributed to the stability of its SO-responsive TK-linkers. After internalization into tumor cells, SO was generated through the photoactivation of TK-$PPE_{Ce6\&DOX}$ under precise 660 nm laser irradiation, and resulted in the cleavage of the TK-linkers. The disassembled TK-$PPE_{Ce6\&DOX}$ allowed DOX to achieve boosted release and further photo-triggered chemotherapy. The cellular evaluations confirmed that TK-$PPE_{Ce6\&DOX}$ had efficient lethal effect on tumor cells. This study provided a promising prospect for clinical on-demand chemotherapy by highly-controllable nanoparticles with superior therapeutic effect for cancers.

Conflicts of interest

The authors have declared that no competing interests exist.

Acknowledgements

This research was funded by the Open Project of Key Laboratory of Biomedical Engineering of Guangdong Province (KLBEMGD201703) and Tianjin Medical University General Hospital (ZYYFY2016041).

References

1 D. E. Dolmans, D. Fukumura and R. K. Jain, Photodynamic therapy for cancer, *Nat. Rev. Cancer*, 2003, **3**(5), 380–387, DOI: 10.1038/nrc1071.

2 A. Z. Wang, R. Langer and O. C. Farokhzad, Nanoparticle Delivery of Cancer Drugs, *Annu. Rev. Med.*, 2012, **63**(1), 185–198, DOI: 10.1146/annurev-med-040210-162544.

3 T. M. Allen and P. R. Cullis, Liposomal drug delivery systems: from concept to clinical applications, *Adv. Drug Deliv. Rev.*, 2013, **65**(1), 36–48, DOI: 10.1016/j.addr.2012.09.037.

4 J. Li, C. Sun, W. Tao, Z. Cao, H. Qian, X. Yang and J. Wang, Photoinduced PEG deshielding from ROS-sensitive linkage-bridged block copolymer-based nanocarriers for on-demand drug delivery, *Biomaterials*, 2018, **170**, 147–155, DOI: 10.1016/j.biomaterials.2018.04.015.

5 Y. Matsumura and H. Maeda, A new concept for macromolecular therapeutics in cancer chemotherapy: mechanism of tumoritropic accumulation of proteins and the antitumor agent smancs, *Cancer Res.*, 1986, **46**, 6387–6392, DOI: 10.1016/0304-3835(86)90075-3.

6 D. Peer, J. M. Karp, S. Hong, O. C. Farokhzad, R. Margalit and R. Langer, Nanocarriers as an emerging platform for cancer therapy, *Nat. Nanotechnol.*, 2007, **2**(12), 751–760, DOI: 10.1038/nnano.2007.387.

7 S. S. Lucky, K. C. Soo and Y. Zhang, Nanoparticles in Photodynamic Therapy, *Chem. Rev.*, 2015, **115**(4), 1990–2042, DOI: 10.1021/cr5004198.

8 Y. Luo, H. Wu, C. Feng, K. Xiao, X. Yang, Q. Liu, T. Y. Lin, H. Zhang, J. H. Walton, Y. Ajena, Y. Hu, K. S. Lam and Y. Li, One-Pot" Fabrication of Highly Versatile and Biocompatible Poly(vinyl alcohol)-porphyrin-based Nanotheranostics, *Theranostics*, 2017, **7**(16), 3901–3914, DOI: 10.7150/thno.20190.

9 C. He, D. Liu and W. Lin, Self-assembled core–shell nanoparticles for combined chemotherapy and photodynamic therapy of resistant head and neck cancers, *ACS Nano*, 2015, **9**(1), 991–1003, DOI: 10.1021/nn506963h.

10 X. Xu, P. E. Saw, W. Tao, Y. Li, X. Ji, S. Bhasin, Y. Liu, D. Ayyash, J. Rasmussen and M. Huo, ROS-responsive polyprodrug nanoparticles for triggered drug delivery and effective cancer therapy, *Adv. Mater.*, 2017, **29**(33), 1700141, DOI: 10.1002/adma.201700141.

11 H. Han, D. Valdepérez, Q. Jin, B. Yang, Z. Li, Y. Wu, B. Pelaz, W. J. Parak and J. Ji, Dual enzymatic reaction-assisted gemcitabine delivery systems for programmed pancreatic cancer therapy, *ACS Nano*, 2017, **11**(2), 1281–1291, DOI: 10.1021/acsnano.6b05541.

12 Y. Wang, L. Zhu, Y. Wang, L. Li, Y. Lu, L. Shen and L. W. Zhang, Ultrasensitive GSH-responsive ditelluride-containing poly(ether-urethane) nanoparticles for controlled drug release, *ACS Appl. Mater. Interfaces*, 2016, **8**(51), 35106–35113, DOI: 10.1021/acsami.6b14639.

13 Y. Fan, C. Li, F. Li and D. Chen, pH-activated size reduction of large compound nanoparticles for *in vivo* nucleus-targeted drug delivery, *Biomaterials*, 2016, **85**, 30–39, DOI: 10.1016/j.biomaterials.2016.01.057.

14 P. L. Bedard, A. R. Hansen, M. J. Ratain and L. L. Siu, Tumour heterogeneity in the clinic, *Nature*, 2013, **501**(7467), 355–364, DOI: 10.1038/nature12627.

15 G. Song, D. B. Darr, C. M. Santos, M. Ross, A. Valdivia, J. L. Jordan, B. R. Midkiff, S. Cohen, N. Nikolaishvili-Feinberg and C. R. Miller, Effects of tumor microenvironment heterogeneity on nanoparticle disposition and efficacy in breast cancer tumor models, *Clin. Cancer Res.*, 2014, **20**(23), 6083–6095, DOI: 10.1158/1078-0432.CCR-14-0493.

16 S. Bonnet, Shifting the light activation of metallodrugs to the red and near-infrared region in anticancer phototherapy, *Comments Inorg. Chem.*, 2015, **35**(4), 179–213, DOI: 10.1080/02603594.2014.979286.

17 Z. Cao, Y. Ma, C. Sun, Z. Lu, Z. Yao, J. Wang, D. Li, Y. Yuan and X. Yang, ROS-sensitive polymeric nanocarriers with red light-activated size shrinkage for remotely controlled drug release, *Chem. Mater.*, 2018, **30**(2), 517–525, DOI: 10.1021/acs.chemmater.7b04751.

18 M. Wang, S. Sun, C. I. Neufeld, B. Perez-Ramirez and Q. Xu, Reactive oxygen species-responsive protein modification and its intracellular delivery for targeted cancer therapy, *Angew. Chem. Int. Ed.*, 2014, **53**(49), 13444–13448, DOI: 10.1002/anie.201407234.

19 V. Deepagan, S. Kwon, D. G. You, W. Um, H. Ko, H. Lee, D.-G. Jo, Y. M. Kang and J. H. Park, In situ diselenide-crosslinked polymeric micelles for ROS-mediated anticancer drug delivery, *Biomaterials*, 2016, **103**, 56–66, DOI: 10.1016/j.biomaterials.2016.06.044.

20 S. Hackbarth, W. Islam, J. Fang, V. Subr, B. Roder, T. Etrych and H. Maeda, Singlet oxygen phosphorescence detection in vivo identifies PDT-induced anoxia in solid tumors,

Photochem. Photobiol. Sci., 2019, **18**(6), 1304–1314, DOI: 10.1039/c8pp00570b.

21 B. Liu, T. J. Farrell and M. S. Patterson, A dynamic model for ALA-PDT of skin: simulation of temporal and spatial distributions of ground-state oxygen, photosensitizer and singlet oxygen, *Phys. Med. Biol.*, 2010, **55**(19), 5913–5932, DOI: 10.1088/0031-9155/55/19/019.

22 C.-Y. Sun, Z. Cao, X.-J. Zhang, R. Sun, C.-S. Yu and X. Yang, Cascade-amplifying synergistic effects of chemo-photodynamic therapy using ROS-responsive polymeric nanocarriers, *Theranostics*, 2018, **8**(11), 2939, DOI: 10.7150/thno.24015.

23 B. Zhang, C. Xu, C. Sun and C. Yu, Polyphosphoester-Based Nanocarrier for Combined Radio-Photothermal Therapy of Breast Cancer, *ACS Biomater. Sci. Eng.*, 2019, **5**(4), 1868–1877, DOI: 10.1021/acsbiomaterials.9b00051.

24 Y. Sun, X. Du, J. He, J. Hu, M. Zhang and P. Ni, Dual-responsive core-crosslinked polyphosphoester-based nanoparticles for pH/redox-triggered anticancer drug delivery, *J. Mater. Chem. B*, 2017, **5**(20), 3771–3782, DOI: 10.1039/C7TB00440K.

25 S. Lv, Z. Tang, M. Li, J. Lin, W. Song, H. Liu, Y. Huang, Y. Zhang and X. Chen, Co-delivery of doxorubicin and paclitaxel by PEG-polypeptide nanovehicle for the treatment of non-small cell lung cancer, *Biomaterials*, 2014, **35**(23), 6118–6129, DOI: 10.1016/j.biomaterials.2014.04.034.

26 W. Li, C. Zheng, Z. Pan, C. Chen, D. Hu, G. Gao, S. Kang, H. Cui, P. Gong and L. Cai, Smart hyaluronidase-actived theranostic micelles for dual-modal imaging guided photodynamic therapy, *Biomaterials*, 2016, **101**, 10–19, DOI: 10.1016/j.biomaterials.2016.05.019.

27 T. Ohyashiki, M. Nunomura and T. Katoh, Detection of superoxide anion radical in phospholipid liposomal membrane by fluorescence quenching method using 1,3-diphenylisobenzofuran, *Biochim. Biophys. Acta, Biomembr.*, 1999, **1421**(1), 131–139, DOI: 10.1016/S0005-2736(99)00119-4.

28 D. Mishra, S. Wang, S. Michel, G. Palui, N. Zhan, W. Perng, Z. Jin and H. Mattoussi, Photochemical transformation of lipoic acid-based ligands: probing the effects of solvent, ligand structure, oxygen and pH, *Phys. Chem. Chem. Phys.*, 2018, **20**(6), 3895–3902, DOI: 10.1039/C7CP06350D.

29 Y.-C. Wang, S.-Y. Shen, Q.-P. Wu, D.-P. Chen, J. Wang, G. Steinhoff and N. Ma, Block copolymerization of ε-caprolactone and 2-methoxyethyl ethylene phosphate initiated by aluminum isopropoxide: synthesis, characterization, and kinetics, *Macromolecules*, 2006, **39**(26), 8992–8998, DOI: 10.1021/ma061821c.

30 C.-S. Xiao, Y.-C. Wang, J.-Z. Du, X.-S. Chen and J. Wang, Kinetics and mechanism of 2-ethoxy-2-oxo-1,3,2-dioxaphospholane polymerization initiated by stannous octoate, *Macromolecules*, 2006, **39**(20), 6825–6831, DOI: 10.1021/ma0615396.

31 M. K. Kiesewetter, E. J. Shin, J. L. Hedrick and R. M. Waymouth, Organocatalysis: opportunities and challenges for polymer synthesis, *Macromolecules*, 2010, **43**(5), 2093–2107, DOI: 10.1021/ma9025948.

32 S. Zhang, A. Li, J. Zou, L. Y. Lin and K. L. Wooley, Facile synthesis of clickable, water-soluble, and degradable polyphosphoesters, *ACS Macro Lett.*, 2012, **1**(2), 328–333, DOI: 10.1021/mz200226m.

33 J. Hu, J. He, D. Cao, M. Zhang and P. Ni, Core cross-linked polyphosphoester micelles with folate-targeted and acid-cleavable features for pH-triggered drug delivery, *Polym. Chem.*, 2015, **6**(17), 3205–3216, DOI: 10.1039/b000000x.

34 V. V. Rostovtsev, L. G. Green, V. V. Fokin and K. B. Sharpless, A stepwise huisgen cycloaddition process: copper (I)-catalyzed regioselective "ligation" of azides and terminal alkynes, *Angew. Chem. Int. Ed.*, 2002, **41**(14), 2596–2599, DOI: 10.1002/1521-3773(20020715)41:143.0.CO;2-4.

35 Y. Chen, L. Yu, B. Zhang, W. Feng, M. Xu, L. Gao, N. Liu, Q. Wang, X. Huang and P. Li, Design and Synthesis of Biocompatible, Hemocompatible, and Highly Selective Antimicrobial Cationic Peptidopolysaccharides via Click Chemistry, *Biomacromolecules*, 2019, **20**(6), 2230–2240, DOI: 10.1021/acs.biomac.9b00179.

36 S. Cajot, N. Lautram, C. Passirani and C. Jérôme, Design of reversibly core cross-linked micelles sensitive to reductive environment, *J. Controlled Release*, 2011, **152**(1), 30–36, DOI: 10.1016/j.jconrel.2011.03.026.

37 Z. Zhang, L. Yin, C. Tu, Z. Song, Y. Zhang, Y. Xu, R. Tong, Q. Zhou, J. Ren and J. Cheng, Redox-responsive, core cross-linked polyester micelles, *ACS Macro Lett.*, 2013, **2**(1), 40–44, DOI: 10.1021/mz300522n.

38 Y.-Y. Yuan, Y.-C. Wang, J.-Z. Du and J. Wang, Synthesis of amphiphilic ABC 3-miktoarm star terpolymer by combination of ring-opening polymerization and "click" chemistry, *Macromolecules*, 2008, **41**(22), 8620–8625, DOI: 10.1021/ma801452n.

39 N. V. Tsarevsky, S. A. Bencherif and K. Matyjaszewski, Graft copolymers by a combination of ATRP and two different consecutive click reactions, *Macromolecules*, 2007, **40**(13), 4439–4445, DOI: 10.1021/ma070705m.

40 K. Liu, R. Xing, Q. Zou, G. Ma, H. Möhwald and X. Yan, Simple peptide-tuned self-assembly of photosensitizers towards anticancer photodynamic therapy, *Angew. Chem. Int. Ed.*, 2016, **55**(9), 3036–3039, DOI: 10.1002/anie.201509810.

41 M. Wozniak, F. Tanfani, E. Bertoli, G. Zolese and J. Antosiewicz, A new fluorescence method to detect singlet oxygen inside phospholipid model membranes, *Biochim. Biophys. Acta Lipids Lipid. Metabol.*, 1991, **1082**(1), 94–100, DOI: 10.1016/0005-2760(91)90304-Z.

42 P. Pei, C. Sun, W. Tao, J. Li, X. Yang and J. Wang, ROS-sensitive thioketal-linked polyphosphoester-doxorubicin conjugate for precise phototriggered locoregional chemotherapy, *Biomaterials*, 2019, **188**, 74–82, DOI: 10.1016/j.biomaterials.2018.10.010.

43 L. Liu, T. Li, Z. Ruan, P. Yuan and L. Yan, Reduction-sensitive polypeptide nanogel conjugated BODIPY-Br for NIR imaging-guided chem/photodynamic therapy at low light and drug dose, *Mater. Sci. Eng. C*, 2018, **92**, 745–756, DOI: 10.1016/j.msec.2018.07.034.

44 A. El-Zawahry, J. McKillop and C. Voelkel-Johnson, Doxorubicin increases the effectiveness of Apo2L/TRAIL for tumor growth inhibition of prostate cancer xenografts, *BMC Canc.*, 2005, **5**(1), 2, DOI: 10.1186/1471-2407-5-2.

45 I. Müller, A. Jenner, G. Bruchelt, D. Niethammer and B. Halliwell, Effect of concentration on the cytotoxic mechanism of doxorubicin—apoptosis and oxidative DNA damage, *Biochem. Biophys. Res. Commun.*, 1997, **230**(2), 254–257, DOI: 10.1006/bbrc.1996.5898.

46 S. Chen, A.-C. Cheng, M.-S. Wang and X. Peng, Detection of apoptosis induced by new type gosling viral enteritis virus *in vitro* through fluorescein annexin V-FITC/PI double labeling, *World J. Gastroenterol.*, 2008, **14**(14), 2174, DOI: 10.3748/wjg.14.2174.